JOURNAL OF SPACECRAFT AND ROCKETS
Vol. 34, No. 4, July–August 1997

# Flight Control Augmentors for Aft-Center-of-Gravity Launch Vehicles

Chris Barret*
*NASA Marshall Space Flight Center, Huntsville, Alabama 35812*

**The author presents the details of the designed flight control augmentors, the wind tunnel test programs conducted at the NASA Marshall Space Flight Center, and the stability and control analyses results for the augmented launch vehicle. Forward and aft, all-movable, blunt-trailing-edge flight control augmentors have been designed and wind tunnel tested to provide the required flight control augmentation for a family of aft-center-of-gravity launch vehicles that could not be adequately controlled using engine gimbaling alone. Previous publications have presented the other parts of this comprehensive research project: the developmental stages of the program, the comprehensive reviews of our national heritage of launch vehicles that have used aerodynamic surfaces and current use of these by other nations, and a state-of-the-art assessment of smart materials and advanced composites directly applicable to the innovative design of the flight control augmentors. It is shown that the blunt-trailing-edge design provides the maximum flight control augmentation.**

## Nomenclature

$AT$ = aerodynamic torque, ft-lb
$CR$ = control ratio, nondimensional
$CT$ = control torque, ft-lb
$C_A$ = coefficient of axial force
$C_l$ = coefficient of rolling moment
$C_m$ = coefficient of pitching moment
$C_{m_q} + C_{m_{\dot\alpha}}$ = pitch damping derivatives
$C_{m_\alpha}$ = gradient of coefficient of pitching moment, deg$^{-1}$, $\partial C_m/\partial\alpha$
$C_N$ = coefficient of normal force
$C_{N_\alpha}$ = gradient of coefficient of normal force, deg$^{-1}$, $\partial C_N/\partial\alpha$
$C_{N_{\alpha_F}}$ = flight control augmentor (FCA) gradient of coefficient of normal force, deg$^{-1}$, $\partial C_{N_F}/\partial\alpha$
$C_n$ = coefficient of yawing moment
$C_Y$ = coefficient of side force
$d$ = reference length, which for a launch vehicle (LV) is the diameter of the major portion of the fuselage and is called a caliber, ft
$E$ = number of engines
$I_y$ = moment of inertia about $y$ axis, slug · ft$^2$
$l_{\text{c.p.}}$ = moment arm from center of gravity to center of pressure, ft
$l_E$ = moment arm from center of gravity to engine gimbal plane, ft
$l_F$ = moment arm from center of gravity to aerodynamic center of FCA, ft
$N$ = normal force, lb
$N_F$ = normal force provided by FCAs, lb
$Q$ = dynamic pressure, lb/ft$^2$
$S$ = reference area, which for an LV is the cross-sectional area of the major length of fuselage, ft$^2$
$S_F$ = planform area of one FCA, ft$^2$
$T$ = thrust per engine, lb
$t$ = time to half or double amplitude of oscillation, s
$u$ = forward flight velocity, ft/s
$X_{\text{c.g.}}$ = distance from moment reference point (MRP) to center of gravity, ft
$X_{\text{c.p.}}$ = distance from MRP to center of pressure, ft
$\alpha$ = angle of attack, deg
$\beta$ = angle of sideslip, deg
$\delta_E$ = engine gimbal deflection angle, deg
$\delta_F$ = deflection angle of the all-movable FCA, deg
$\Lambda$ = planform sweep angle

Received Nov. 21, 1996; revision received March 28, 1997; accepted for publication March 28, 1997. 

*Aerospace Engineer, ED13. Senior Member AIAA.

## Introduction

THE Space Shuttle was only the first step in achieving routine access to space. Recently, a whole spectrum of new launch vehicles (LVs) for space transportation has been studied at the NASA Marshall Space Flight Center (MSFC). In all future LV designs, decreasing the structural weight will always be of great concern. This is tantamount to increased payload capability, which in turn means reduced cost per pound to orbit. One very significant increase in payload capability has been defined in an LV family studied. It has been shown that sizable weight savings can be realized by a rearrangement of the internal propellant tanks. Studies have been conducted both at MSFC and at Lockheed Martin, maker of the Space Shuttle external tank (ET), which show that a very substantial weight can be saved by inverting the relative positions of the liquid hydrogen ($LH_2$) and the liquid oxygen (LOX) propellant tanks.

As the vehicle sits on the launch pad in the conventional configuration, the heavier LOX tank is located on top of the lighter $LH_2$ tank. This requires a heavy structural member between the two tanks to prevent the $LH_2$ tank from being crushed. This configuration also requires large, long, heavy, and even drag-producing LOX feedlines running the length of the vehicle on the exterior fuselage. If the relative position of the propellant tanks is inverted, both the heavy structural separation member and the long LOX feedlines could be deleted. This configuration would also reduce the fueling time. Although the structures community was elated with this finding, the LOX-tank-aft configuration gave the vehicle an aft-center-of-gravity (c.g.) location that surfaced controllability concerns. In the conventional configuration the LV is controlled in the ascent trajectory by the gimbaling of its rocket engines. However, the resulting aft-c.g.-configured LV would not be adequately controllable with engine gimbaling alone. It is known that the controllability of an aft-c.g. LV is decreased. Today, more aft-c.g. LVs are appearing because of the larger numbers of aft engines and added strap-on boosters. Therefore, in the new spectrum of LVs being considered, when the available control authority has been determined to be inadequate or marginal, some means of flight control augmentation is required.

In this research effort the author has proposed that the designed all-movable, blunt-trailing-edge flight control augmentors (FCAs),

possibly incorporating smart materials for small-tab actuation[1] to aid actuation of the FCAs and advanced composites for reduced thermal protection requirements, provide the required flight control augmentation for the aft-c.g.-configured LV, especially when needed most in the ascent trajectory, during maximum dynamic pressure (max $Q$). As seen in Ref. 2, though stationary aerodynamic surfaces have been used in the past in the Saturn series of LVs, and though there have been some small movable tip controls on some earlier LVs, all-movable FCAs have not been used on a large Saturn-class LV to augment engine gimbaling to the author's knowledge. The designed FCAs can also be used in the marginal control configuration to enhance controllability, as load alleviators, to reduce engine gimbaling requirements, to provide engine actuator failure protection, and to enhance crew safety and vehicle reliability by providing more control in engine-out events.

The added control capability through the use of the FCAs allows greater tolerance of wind magnitudes and a minimization of bending moments on the vehicle during both liftoff and ascent. Conventionally, the LV aerodynamic loads during ascent are alleviated by turning the vehicle into the wind, thereby reducing the flight $\alpha$ and/or $\beta$. Thus, load relief is accomplished at the expense of trajectory deviation. Load relief control is most necessary when the LV experiences max $Q$ and the aerodynamic loads are greatest. The time during the max $Q$ portion of the trajectory happens to be when the FCAs would provide the most significant assistance. For prelaunch, the unfueled vehicle on the pad must withstand peak winds of 75 kn, and fueled at liftoff, peak winds of 50 kn. The environmental disturbances are multiplied by 1.5 to allow for von Kármán vortex-shedding effects.

Wind profiles show that the greatest steady wind speeds occur between 20,000 and 60,000 ft with a gust overshoot of up to 50%. The more the engines are required to gimbal, the more engineering design and cost is involved in having the propellant ducts move with the gimbal action while maintaining a full flow of fuel. The extension, compression, and torsion of the propellant ducts become limiting factors of engine gimbaling. Thus, the designed FCAs of this research provide not only the required control augmentation but a plethora of additional significant benefits.

Figure 1 shows the scope of this comprehensive research project. Previous publications[1–6] have presented the developmental stages of the program; comprehensive reviews of our national heritage of LVs that have used aerodynamic surfaces and current use of these by other nations; and a state-of-the-art assessment of smart materials and advanced composites directly applicable to the innovative design of the FCAs. This paper presents details of the designed FCAs, the wind tunnel test program conducted at MSFC, and the stability and control analyses.

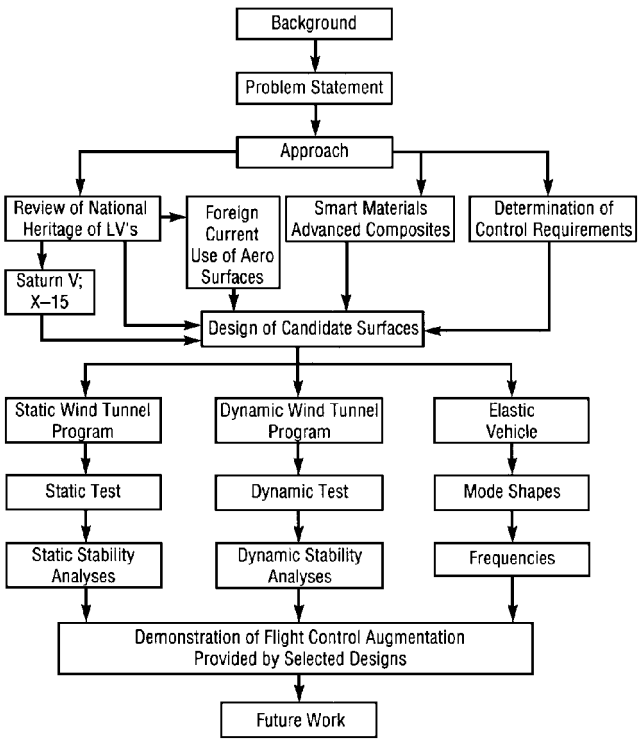


**Fig. 1 Flowchart of conducted research.**

## Control Requirements

For this research effort, an experimental LV has been selected, which is an expendable vehicle very similar to the Saturn V in many respects and 74% of its length (with a length of 269.3 ft) and propelled by six bipropellant rocket engines, each providing 583,000 lb of vacuum thrust. The positions of the LOX tank and the $LH_2$ tank have been interchanged, the LOX feedlines have been deleted, and the biconic nose has been redesigned to a 1.2-caliber ogive nose to better accommodate forward-located canard FCAs by providing a cleaner and more uniform flow. Then, based on the review of our national heritage of LVs using aerodynamic surfaces, the review of the X-15 and Saturn series design concepts,[2] the survey of current use of aerodynamic surfaces by other nations, the generated mass properties and trajectory data for the aft-c.g. experimental LV, the original aerodynamic data, the U.S. Air Force Stability and Control DATCOM[7] as a preliminary design tool, and a control requirement analysis, a set of candidate FCAs were designed for the wind tunnel test program.

The traditional LV control requirement at MSFC is to have the ratio of the control torque to the aerodynamic torque be greater than or equal to 1.5, i.e., the LV is to have at least 1.5 times as much control authority over the vehicle as the pitch-up destabilizing aerodynamic moment. That is,

$$CR = (CT/AT) \geq 1.5 \tag{1}$$

This control requirement is used to size the designed LV FCAs. From Fig. 2, using force and moment equations, it can be seen that, about the c.g.,

$$CT = T \sin \delta_E(E) l_E \tag{2}$$

$$AT = N\, l_{\text{c.p.}} = C_{N_\alpha}\, \alpha\, Q\, S\, l_{\text{c.p.}} = C_N\, Q\, S\, l_{\text{c.p.}} \tag{3}$$

$$l_{\text{c.p.}} = X_{\text{c.p.}} - X_{\text{c.g.}} \tag{4}$$

Thus, Eq. (1) becomes

$$CR = \frac{T \sin \delta_E(E) l_E}{C_{N_\alpha}(\alpha)(Q)(S)\, l_{\text{c.p.}}} \geq 1.5 \tag{5}$$

It can be seen that, about the moment reference point (MRP),

$$AT = C_{N_\alpha}\, \alpha Q S X_{\text{c.p.}} = C_m Q S d = C_{m_\alpha}\, \alpha Q S d \tag{6}$$

Therefore,

$$AT = C_{N_\alpha}\, \alpha Q S \left(C_{m_\alpha}/C_{N_\alpha}\right) d = \left(C_{m_\alpha} Q\right) \alpha (\pi\, d^3/4) \tag{7}$$

Equation (7) shows that the maximum $AT$, for a fixed $\alpha$, occurs when $C_{m_\alpha} Q$ is a maximum.

When an LV flies through its ascent trajectory, the traditional critical point, from an aerodynamic loads standpoint, is near max $Q$. LV control systems and structures are designed around this critical point, and LV trajectories are shaped accordingly. For the experimental LV, Fig. 3 shows the variation of critical parameters during ascent, and Table 1 lists the values used at max $Q$. Substituting the values from Table 1 into Eq. (5) yields a control ratio of 1.3. This is inadequate controllability, since the minimum requirement is 1.5.

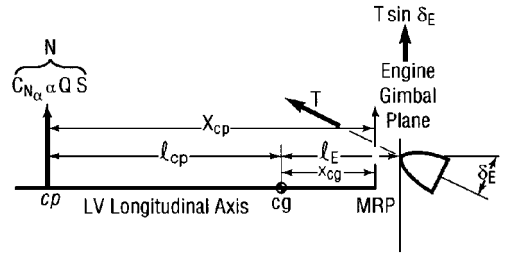


**Fig. 2 Aerodynamic torque vs engine gimbal torque.**

## Flight Control Augmentor Design

Using Eq. (1) to size the all-movable FCA planform that will provide the required controllability,

$$CR = \frac{CT + N_F l_F}{AT} = \frac{T \sin\delta_E\,(E) l_E + C_{N_{\alpha_F}}\,(\alpha + \delta_F) Q\, 2 S_F\, l_F}{C_{N_\alpha}\,\alpha Q S l_{\text{c.p.}}} \geq 1.5 \quad (8)$$

It is assumed here that the ratio of local dynamic pressures at the FCA location is very close to 1, that the aerodynamic center (a.c.) of the FCA is near the quarter-chord location (which is a conservative assumption), and that the moment about the FCA ($C_{m_{\text{a.c.}_F}}$) is near zero, i.e., that the FCA is symmetrical without camber. The FCAs augment the control torque by shifting the LV c.p. aft, thereby reducing the moment arm of the resultant normal force on the vehicle. The c.p. is the point of no moment, whereas the a.c. is the point where the moment is independent of $\alpha$, i.e., where $C_{m_\alpha}$ equals zero. For a symmetrical vehicle c.p. = a.c. The c.p. location is of vital concern in flight stability and control, since it determines the aerodynamic moment arm.

**Table 1 Experimental LV values**

| | |
|---|---|
| max $Q$ | 639.9 psf |
| $T$ | 520,512 lb/engine |
| $E$ | 6 |
| $M$ | 1.41 |
| $S$ | 597.56 ft$^2$ |
| $d$ | 27.58 ft |
| $C_{N_\alpha}$ | 0.057153 |
| $C_{m_\alpha}$ | 0.321070 |
| $X_{\text{c.g.}}$ | 52.98 ft |
| $l_E$ | 53.4 ft |
| $\delta_E$ | 4 deg[a] |
| $\alpha$ | 4 deg[b] |
| $X_{\text{c.p.}}$ | 5.62 calibers = 155 ft |
| $l_{\text{c.p.}}$ | 101.52 ft |

[a]Usual for routine control; 8 deg is also possible.
[b]Based on the maximum used during Saturn V flights.

To solve Eq. (8), values for $C_{N_{\alpha_F}}$ and $l_{\text{c.p.}}$ are needed. From previous work with Saturn V aerodynamic data, the value of $C_{N_{\alpha_F}}$ as a function of Mach number has been found: $C_{N_{\alpha_F}} = 0.1102$/deg. When these values were substituted into Eq. (8) for the experimental LV, the following was obtained:

| $\delta_F$, deg | $S_F$, ft$^2$ | Engine-out $S_F$, ft$^2$ |
|---|---|---|
| 2 | 44 | 95 |
| | | Choose 80 |
| 4 | 33 | 71 |

A planform area of 80 ft$^2$ is chosen not only to move the c.p. aft and thereby improve stability and control but also to accommodate a very far-aft c.g. and an engine out. Choosing 80 ft$^2$ means that in an engine-out event the LV control requirements would be met with less than 4 deg of FCA deflection. The FCAs together with the thrust vector control then provide the required control authority.

After an aerodynamic surface has been sized, the next step is to decide on a planform shape. Since the experimental LV is expendable, simple planform designs were desired for ease of fabrication.

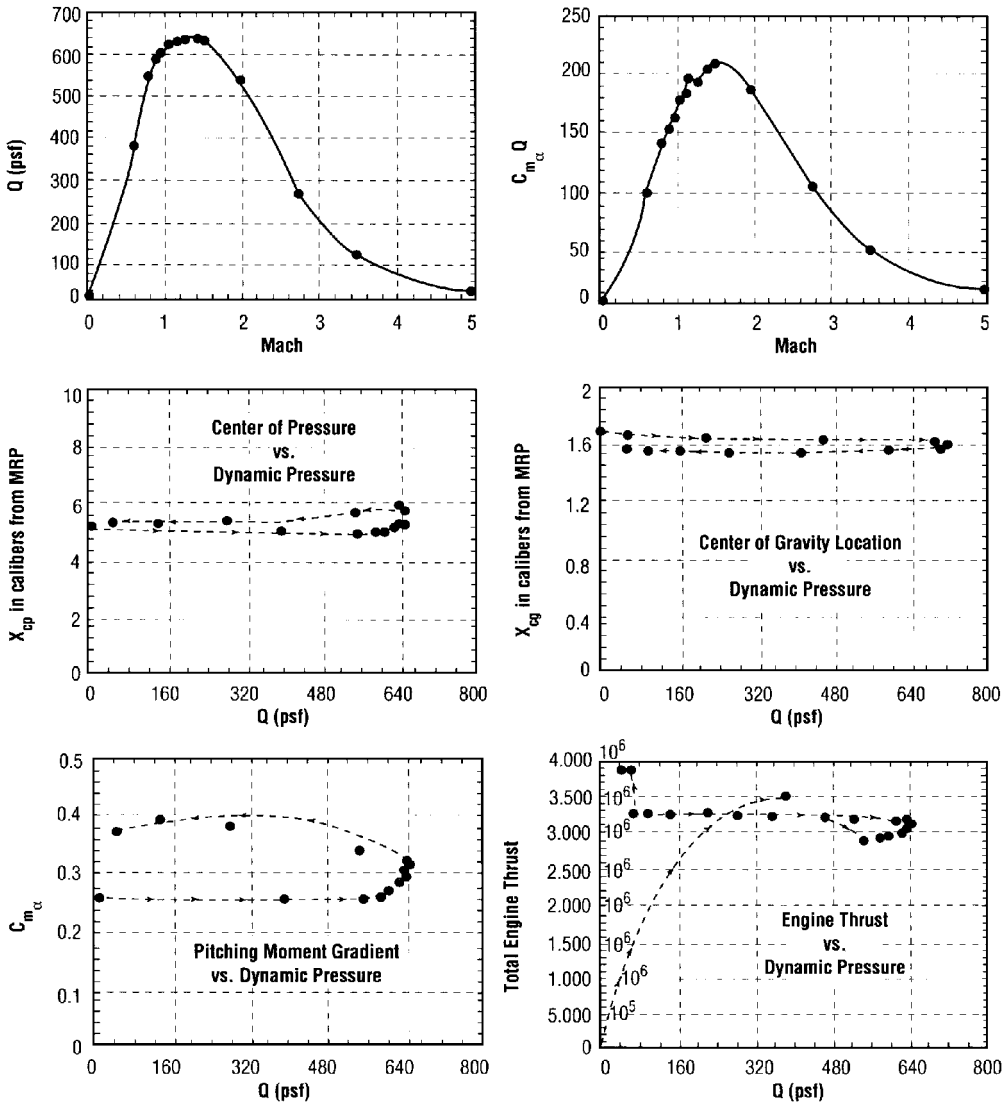


**Fig. 3 Variation of ascent parameters for the experimental LV.**

Therefore, the only other significant design issues to address were the operational speed regimes, the aspect ratio $A$, the leading edge (LE) sweep angle $\Lambda$, the taper ratio $\tau$, the airfoil, and the airfoil thickness-to-chord $(t/c)$ ratio. During its ascent flight, the experimental LV flies through three speed regimes: subsonic, transonic, and supersonic. It has been established that the FCAs will provide the greatest assistance to the LV during the time when $C_{m_\alpha} Q$ is maximum. Since this is during the supersonic regime, the FCAs were designed for that regime.

All-movable FCAs were chosen because they are known to have an operational advantage in the supersonic regime. In subsonic flow, a trailing edge (TE) effect of a partially movable control surface is felt upstream. In supersonic flow, on the other hand, the forward part of a surface does not feel the effect of a deflected aft portion of a control surface. Thus, if large lift is desired, the entire surface should move. A set of four cruciform FCAs were chosen on the basis of Saturn V success[2] and also on the fact that the experimental LV has four of its six engines located in line with the aft fuselage circumference and hence four engine shrouds, which provide suitable locations for four FCAs.

There are not many basic shapes of supersonic airfoils from which to choose. The basic shapes are the diamond and the lenticular. Part of a detailed study by Wood and Miller[8] showed that the lift generated by the basic diamond and the basic lenticular shapes demonstrated no discernable differences between the two airfoils. Thus, the author has chosen a variety of diamond and lenticular airfoils for the FCA designs that were wind tunnel tested. Whereas drag minimization is a driver in many airfoil designs, it was not in this case. The aerodynamic surface drag of the vehicles studied in Ref. 2 was $<2\%$ of the total vehicle drag. Symmetrical airfoils without camber were chosen. For the experimental LV using a set of four FCAs at 80 ft$^2$ each,

$$\frac{S_F}{S_{\text{wetted}}} = 1.6\% \tag{9}$$

The six bipropellant liquid engines of the experimental LV produce 3,500,400 lb of thrust, and the time of FCA use is 4 min.

Blunt rather than sharp TEs can be used on an LV, since FCA drag is normally $<2\%$ of the total vehicle drag. Blunt TEs have been used successfully in many previous LVs, as cited in Ref. 1. The reasons include avoidance of transonic problems, ease of fabrication, utility for holddown posts, structural rigidity to help prevent flutter, and, in the case of the X-15, for better high-speed directional control.[2] Blunt TEs have also been used to solve transonic problems on French sounding rockets such as the D6 (ONERA).[9] ONERA in France had the transonic problem of shock-induced boundary-layer separation on the downstream part of airfoils used on the base of the first stage. This transonic boundary-layer separation resulted in decreased stability and increased load factors. The transonic problem was corrected by the use of thick TE's, and it was found that the wedge shape experienced no transonic problems and produced much improvement in static flight stability.[9]

Better control effectiveness was what was being sought here for the designed FCAs. As shown in Ref. 1, none of the blunt TE surfaces of the Saturn series moved, so the amount of increased control effectiveness on an LV was not known. Could the increased control effectiveness of the blunt TE achieved on the X-15 be realized on an LV? The blunt TE also helps to avoid some transonic problems of fluctuating $C_m$ and negative local lift due to transonic shocks. The blunt TE was also structurally appealing for possible future insertion of reaction control systems (RCSs) and/or smart actuator mechanisms, in view of the space available in a blunt TE airfoil. Therefore, the FCAs designed incorporate blunt TEs.

There is some preference for triangular planforms for supersonic speeds because of smaller c.p. shifts in going from subsonic to supersonic speeds, more vortex lift, and more negative pitching moments, and there is some preference for trapezoidal planforms for subsonic speeds. However, the recent literature shows that wind tunnel tests are still being used extensively to make final decisions on planform shape parameters and also to increase databases so that current aerodynamic prediction codes can be further refined.

A total of 12 candidate FCAs have been designed for wind tunnel tests: 11 aft FCAs and one forward canard FCA, which are shown in Fig. 4 and described in Table 2. Since the critical design point is supersonic, eight triangular family aft FCAs and a triangular

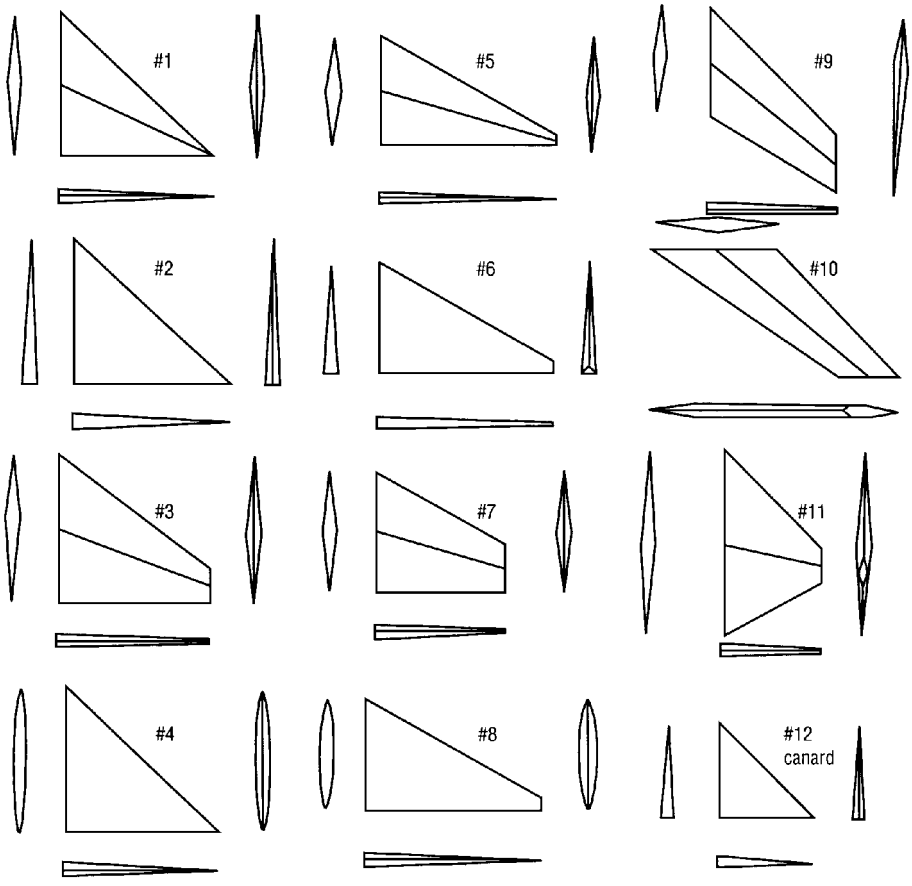


**Fig. 4 Candidate flight control augmentor designs.**

**Table 2 Candidate flight control augmentor design descriptions: 12 FCA designs wind tunnel tested**

| |
|---|
| Four triangular family planforms; LE $\Lambda = 45$ deg; TE = 0 deg |
| One full diamond airfoil (no. 1) |
| One half diamond; blunt TE (no. 2) |
| One full diamond; clipped tip (no. 3) |
| One lenticular airfoil (no. 4) |
| Four triangular family planforms; LE $\Lambda = 30$ deg; TE = 0 deg |
| One full diamond airfoil (no. 5) |
| One half diamond; blunt TE (no. 6) |
| One full diamond; clipped tip (no. 7) |
| One lenticular airfoil (no. 8) |
| One aft swept trapezoidal planform; LE $\Lambda = 45$ deg; TE = 30 deg (no. 9) |
| One forward swept trapezoidal planform; LE $\Lambda = -45$ deg; TE = $-55$ deg (no. 10) |
| One tapered trapezoidal planform; LE $\Lambda = 45$ deg; TE = $-30$ deg (no. 11) |
| One triangular planform canard; half diamond; blunt TE (no. 12) |

canard were chosen. Based on the success of the Saturn IB LV,[2] four FCAs have $\Lambda = 45$ deg; based on that of the Saturn V LV,[2] four FCAs have $\Lambda = 30$ deg. The eight FCAs in the triangular family were all originally true triangles; however, for launch pad logistics (and structural/fabrication considerations) some of the tips were clipped. These clipped-tip designs are of course strictly trapezoids. For comparison with the triangular planform families, an aft-swept, a forward-swept, and a trapezoidal tapered planform, all with diamond airfoils, have been used. Aspect ratios ranged from 1.74 to 5.625. Some options for investigation of further increased control effectiveness could include RCS or jet flaps. The Shuttle aerodynamic flight control surfaces become effective approximately 10 s into the launch ascent trajectory, at which time the dynamic pressure is of sufficient magnitude. Additional and earlier control torque could possibly be provided by the FCAs designed here, if RCS or the jet flap concept were incorporated into the blunt TE.

It is well known that an aerodynamic flight control surface located forward of the c.g. on a flight vehicle normally produces an effect that is destabilizing to its static stability. Although canards cause static instability, they have been used extensively on subsonic and supersonic aircraft and missiles for a variety of reasons. Some advantages provided by canards include production of lift at the nose, high maneuverability due to fast response time, and reduced trim drag in lifting cruise flight. Canard control can be used here to provide negative lift on the nose and a pitch-down torque, which would achieve the control objective.

For the application here, the vortices moving from the canards onto the LV empennage must be considered, as the canard downwash acting on the empennage can reduce the FCA's control effectiveness. The biconic nose of the experimental LV has been redesigned to provide cleaner and more uniform flow in proximity to the canard controls. The longitudinal body station location of the canards is sometimes a tradeoff between 1) distancing from bow and oblique shocks and their effects on the control authority of the canards and 2) the structural advantages of having the canards located at a major bulkhead. The canards have been designed by using linearized supersonic theory for the canard lift coefficient, along with the same moment balance method used above. The designed triangular 32-ft$^2$ canard planforms have blunt TEs and are located two calibers from the tip of the ogive nose.

## Wind Tunnel Test Program

The static stability wind tunnel test program conducted at the NASA MSFC wind tunnel test facility obtained force and moment data, from which the stability derivatives and control derivatives were calculated for the flight stability and control analysis. The tests measured normal, axial, and side forces and pitching, yawing, and rolling moments and were conducted at Mach numbers from 0.2 to 5, $\alpha$ and $\beta$ ranges of $\pm 10$ deg, aft FCA deflections up to 15 deg in 3-deg increments, and forward FCA deflections of up to 30 deg in 5-deg increments. The three forces and three moments were measured on a six-component strain-gauge balance mounted internally in the experimental LV test article. The MSFC wind tunnel used in this research was the 14 × 14-Inch Trisonic Wind Tunnel.[10] The test articles were fabricated from stainless steel to a scale of 0.5% by Dynamic Engineering Incorporated. Figure 5 shows a diagram of the test LV with its 1.2-caliber ogive nose redesign, canard locations, engine shrouds, aft FCAs, balance center, and MRP. The tests were conducted with and without the canard forward FCAs. Table 3 shows wind tunnel operating conditions, and Table 4 shows wind tunnel test data tolerances.

**Table 3 Wind tunnel operating conditions**

| Mach number | Reynolds number, $10^6$/ft | Dynamic pressure, lb/in.$^2$ | Stagnation temperature, °F | Stagnation pressure, lb/in.$^2$ |
|---|---|---|---|---|
| 0.20 | 1.6 | 0.58 | 100 | 22 |
| 0.40 | 3.4 | 2.21 | 100 | 22 |
| 0.80 | 5.5 | 6.47 | 100 | 22 |
| 0.95 | 6.2 | 7.76 | 100 | 22 |
| 1.20 | 6.5 | 9.15 | 100 | 22 |
| 1.46 | 6.0 | 9.49 | 100 | 22 |
| 1.96 | 7.2 | 11.00 | 100 | 30 |
| 2.74 | 4.7 | 6.38 | 140 | 30 |
| 3.48 | 4.8 | 5.15 | 140 | 45 |
| 4.96 | 4.4 | 2.73 | 140 | 80 |

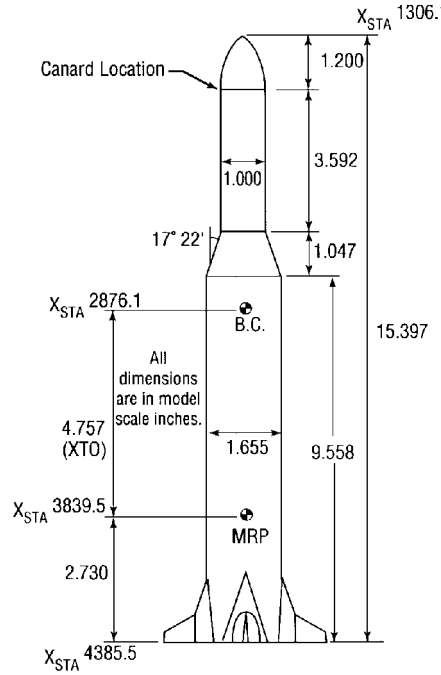


**Fig. 5 Experimental LV wind tunnel model (0.005 scale).**

The dynamic stability wind tunnel test program obtained the damping derivatives for three selected FCAs tested on the experimental LV, for a Mach range of 0.8–2.0, so that dynamic stability characteristics could be compared. Whereas the static stability derivatives are a function of aerodynamic angle, control-surface deflection, and Mach number, the dynamic stability derivatives are a function of aerodynamic angle rates of change, control-surface deflection rates, body rates, and Mach number. Table 5 shows basic dynamic stability derivatives.[11] Oscillation around a fixed axis results in a sum of a purely rotary derivative, and a translational acceleration derivative; e.g., in the longitudinal case, these are $C_{m_q}$ and $C_{m_{\dot{\alpha}}}$, respectively. To facilitate the logistics, a free oscillation with a mechanical release was chosen.

## Stability and Control Analysis

Wind tunnel test data were reduced and linearized to obtain the stability derivatives, i.e., the rates of change of the three forces (normal, axial, and side) and the three moments (pitching, yawing, and rolling) with respect to $\alpha$ and $\beta$,

$$\frac{\partial C_N}{\partial \alpha}, \quad \frac{\partial C_m}{\partial \alpha}, \quad \frac{\partial C_A}{\partial \alpha}, \quad \frac{\partial C_Y}{\partial \beta}, \quad \frac{\partial C_n}{\partial \beta}, \quad \frac{\partial C_l}{\partial \beta}$$

**Table 4 Wind tunnel test data tolerances**

| Quantity | *Strain gauge balance 250* Capacity | Accuracy | Max. loads[a] |
|---|---|---|---|
| Normal force, lb | 200 | +1.00 | 21 |
| Side force, lb | 107 | +0.50 | 4.5 |
| Axial force, lb | 75 | +0.25 | 12 |
| Pitching moment, in. · lb | 200 | +0.99 | 14 |
| Rolling moment, in. · lb | 50 | +0.25 | 1.5 |
| Yawing moment, in. · lb | 107 | +0.49 | 16 |

*Coefficient tolerances*

| Mach no. | Dyn. press. | $C_N$ | $C_m$ | $C_A$ | $C_Y$ | $C_n$ | $C_l$ |
|---|---|---|---|---|---|---|---|
| 0.2 | 0.58 | 0.8057 | 0.4819 | 0.2014 | 0.4028 | 0.2385 | 0.1217 |
| 0.4 | 2.21 | 0.2114 | 0.1265 | 0.0529 | 0.1057 | 0.0626 | 0.0319 |
| 0.8 | 6.47 | 0.0722 | 0.0432 | 0.0181 | 0.0361 | 0.0214 | 0.0109 |
| 0.95 | 7.76 | 0.0602 | 0.0360 | 0.0151 | 0.0301 | 0.0178 | 0.0091 |
| 1.2 | 9.15 | 0.0511 | 0.0305 | 0.0128 | 0.0255 | 0.0151 | 0.0077 |
| 1.46 | 9.49 | 0.0492 | 0.0295 | 0.0123 | 0.0246 | 0.0146 | 0.0074 |
| 1.96 | 11.0 | 0.0425 | 0.0254 | 0.0106 | 0.0212 | 0.0126 | 0.0064 |
| 2.74 | 6.38 | 0.0732 | 0.0438 | 0.0183 | 0.0366 | 0.0217 | 0.0111 |
| 3.48 | 5.15 | 0.0907 | 0.0548 | 0.0227 | 0.0454 | 0.0269 | 0.0137 |
| 4.96 | 2.73 | 0.1712 | 0.1024 | 0.0428 | 0.0856 | 0.0507 | 0.0259 |

[a]Maximum estimated running loads, and not starting loads.

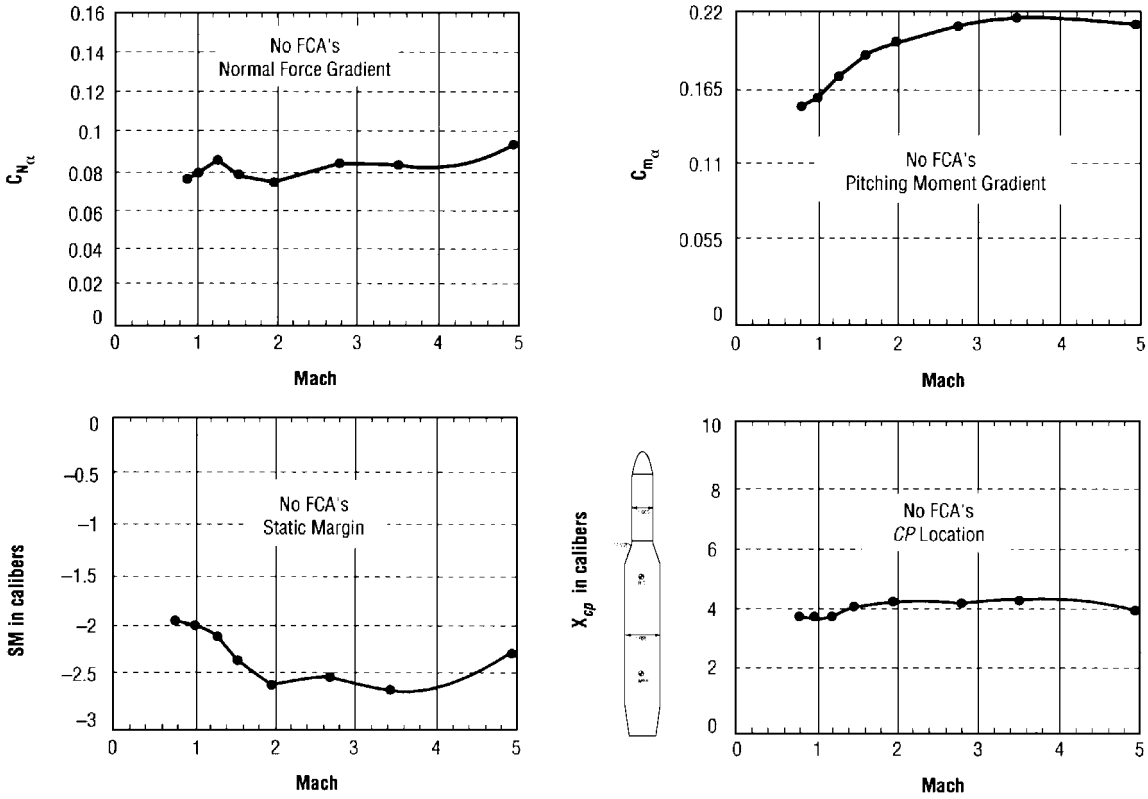


**Fig. 6 Stability results with no flight control augmentors.**

at fixed $M$; the control derivatives, i.e., the rates of change of the forces and the moments with respect to the FCA deflections at fixed $M$,

$$\frac{\partial C_N}{\partial \alpha}, \quad \frac{\partial C_m}{\partial \alpha}, \quad \frac{\partial C_A}{\partial \alpha}, \quad \frac{\partial C_Y}{\partial \beta}, \quad \frac{\partial C_n}{\partial \beta}, \quad \frac{\partial C_l}{\partial \beta}$$

and the c.p. locations $X_{\text{c.p.}}$. The basic stability derivatives were tabulated as slopes of coefficients vs aerodynamic angle curves for fixed FCA deflections. The basic control derivatives were tabulated as slopes of coefficients vs FCA deflection curves for fixed aerodynamic angles.

The criteria for longitudinal static stability of a flight vehicle are

$$C_{m_\alpha} < 0 \tag{10}$$

and for $\alpha_{\text{trim}}$ to be in the flight range of the vehicle. The vehicle $C_{m_\alpha}$ varies with the c.g. position. As the c.g. of a stable vehicle moves farther aft, $C_{m_\alpha}$ becomes less and less negative. When the $C_{m_\alpha}$ has become positive, the vehicle becomes longitudinally unstable. That c.g. location at which $C_{m_\alpha} = 0$ is the neutral point (NP), the a.c. for the entire flight vehicle, that place where the pitching moment is invariant with $\alpha$. The longitudinal static margin (SM) is the quantitative measure of longitudinal static stability used here. The SM is defined as the distance forward of the NP at which the c.g. is located. Of course, when the c.g. is located aft of the NP, the SM is negative and the vehicle is longitudinally unstable. Early LVs were statically stable; today, most are unstable and the control systems provide artificial stability. As an LV's SM becomes more negative, the requirements for control torque increase.

From Eq. (6) or a derivation such as found in Ref. 12, the SM can be defined in terms of the calculated longitudinal static stability parameters,

$$\text{SM} \equiv -\left(C_{m_\alpha}/C_{N_\alpha}\right) \qquad \text{(in calibers)} \tag{11}$$

For the experimental expendable LV in the ascent trajectory, the static flight stability has been assessed. Only the longitudinal static flight stability is presented here. The SMs and the locations of the vehicle c.p. ($X_{c.p.}$) have been determined first for the cases of no FCAs at each Mach number, then for the cases with each of the different FCAs tested at each Mach number but with zero FCA deflection, and finally for each FCA with deflection at each Mach number to assess the improvement in static flight stability and c.p. shift provided by each of the FCA designs during ascent. The FCAs with the greatest aspect ratio had the greatest normal force gradient. Table 6 summarizes the results for the aft FCAs. Figures 6 and 7 show results for the basic experimental LV with no FCAs and with the best FCAs, respectively. Improvements with FCAs ranged from 41 to 72%, with the blunt TE design no. 6 giving the greatest improvement.

**Table 5 Basic dynamic stability derivatives: oscillation around fixed axis**

| Damping derivatives | Cross derivatives | Cross-coupling derivatives |
|---|---|---|
| $C_{l_p} + C_{l_{\dot\beta}} \sin\alpha$ | $C_{l_r} - C_{l_{\dot\beta}} \cos\alpha$ | $C_{l_q} + C_{l_{\dot\alpha}}$ |
| $C_{m_q} + C_{m_{\dot\alpha}}$ | $C_{n_p} + C_{n_{\dot\beta}} \sin\alpha$ | $C_{m_r} - C_{m_{\dot\beta}} \cos\alpha$ |
| $C_{n_r} - C_{n_{\dot\beta}} \cos\alpha$ | | $C_{m_p} + C_{m_{\dot\beta}} \sin\alpha$ |
| | | $C_{n_q} + C_{n_{\dot\alpha}}$ |

**Table 6 Results of aft flight control augmentors**

| FCA no.[a] | SM | Planform design |
|---|---|---|
| No FCAs | −2.0 | |
| 6 | −0.56 | Triangular, 30-deg LE Λ, blunt TE, wedge |
| 8 | −0.75 | Triangular, 30-deg LE Λ, lenticular |
| 5 | −0.77 | Triangular, 30-deg LE Λ, diamond |
| 7 | −0.80 | Triangular, 30-deg LE Λ, diamond, clipped tip |
| 2 | −0.89 | Triangular, 45-deg LE Λ, blunt TE, wedge |
| 1 | −0.92 | Triangular, 45-deg LE Λ, diamond |
| 10 | −0.96 | Forward swept, −45-deg LE Λ, diamond |
| 9 | −1.02 | Aft swept, 45-deg LE Λ, 30-deg TE Λ, diamond |
| 11 | −1.08 | Trapezoidal, 45-deg LE Λ, −30-deg TE Λ, diamond |
| 3 | −1.14 | Triangular, 45-deg LE Λ, diamond, clipped tip |
| 4 | −1.18 | Triangular, 45-deg LE Λ, lenticular |

[a] $\delta = 0$ deg.

With deflection of the FCAs, the pitching-moment coefficient involves more terms,

$$C_m = C_{m_0} + C_{m_\alpha}\,\alpha + C_{m_{\delta_F}}\,\delta_F \tag{12}$$

where

$$C_{m_{\delta_F}} \equiv \frac{\partial C_m}{\partial \delta_F} \equiv \text{FCA control power} \tag{13}$$

The $CR$ has been calculated with no FCAs, with FCAs but no deflection, and last with FCAs and FCA deflection. Figure 8 is the control analysis summary plot, which shows the control ratio for no FCAs, the required amount, and that available through the use of the deflected FCAs. The mere presence of the FCAs with no deflection increased the $CR$ by 46%. For 3 deg of FCA deflection, the $CR$ increased to 346%, and at 9.1 deg FCA deflection, the aerodynamic moment was completely trimmed. The canard forward FCAs were able to trim the vehicle at 5-deg deflection.

Even better results could be achievable by using the FCAs and engine shrouds at 45 deg. When the FCA surfaces are rolled in orientation with respect to the body axes, all four will be working

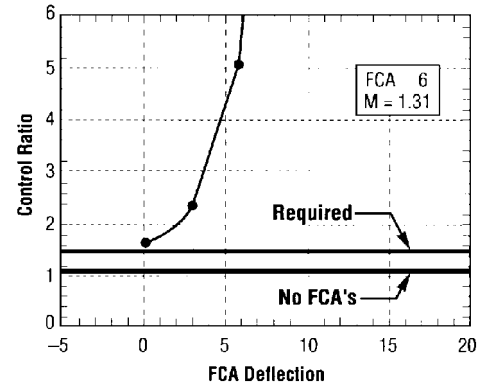


**Fig. 8 Control analysis summary plot.**

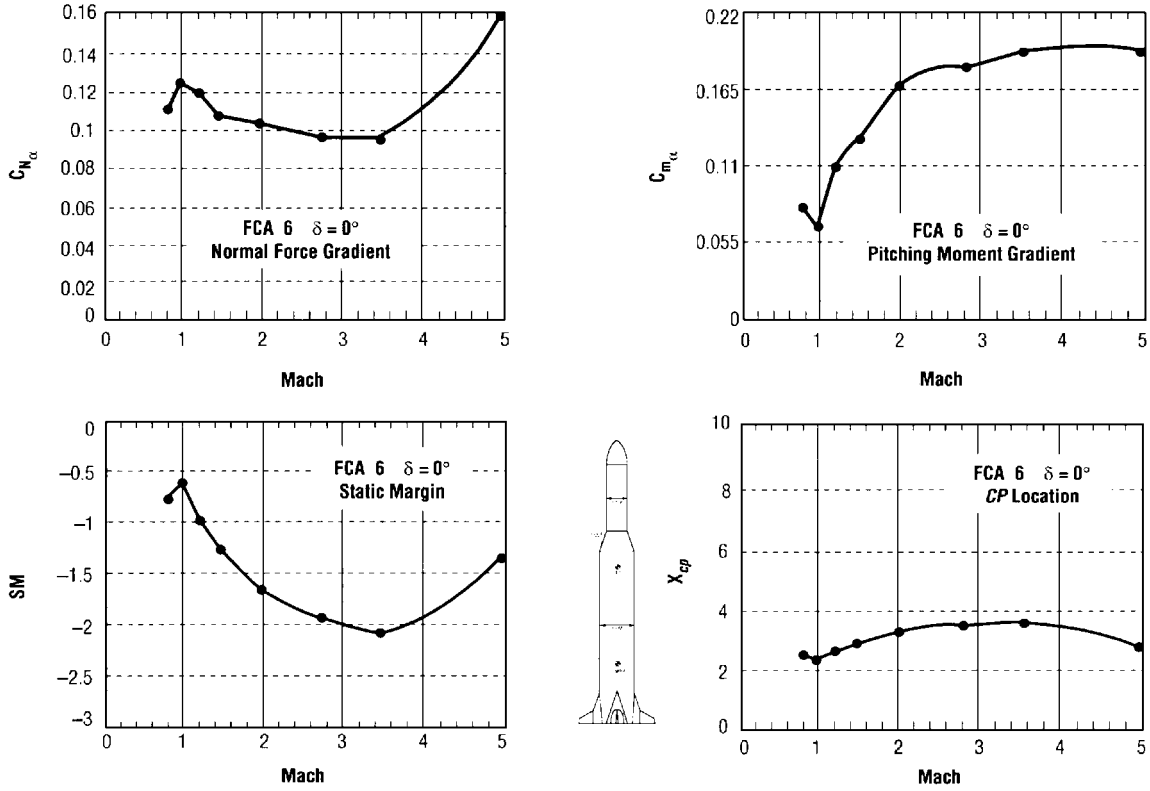


**Fig. 7 Stability results with blunt-trailing-edge flight control augmentors at zero deflection.**

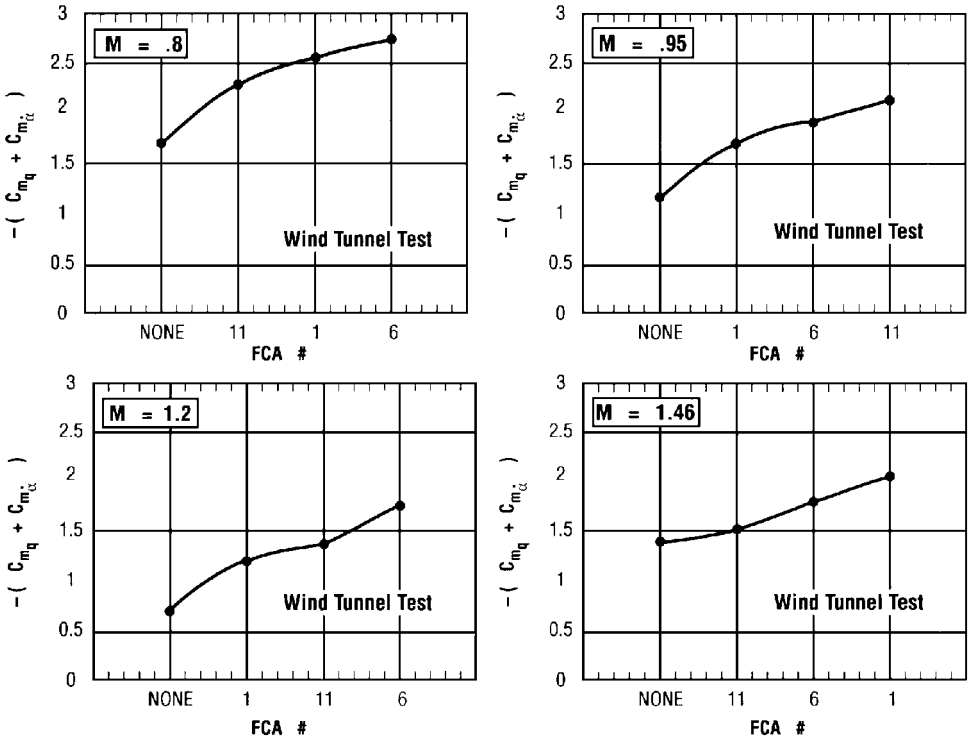


**Fig. 9 Wind tunnel test pitch damping results.**

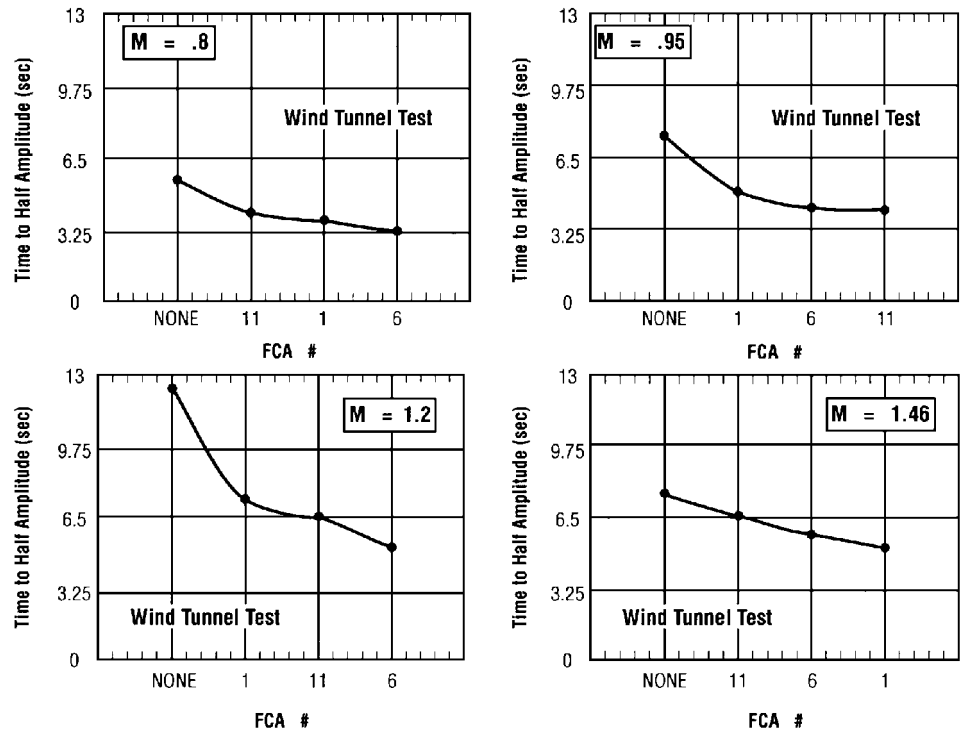


**Fig. 10 Qualitative comparison of short-period mode results.**

in the pitch plane. This orientation is sometimes referred to as the (×) configuration, as opposed to the cruciform (+) configuration. For example,

$$0\,\text{deg}\,(+):\ N_F = 2C_{N_F} QS_F$$
$$45\,\text{deg}\,(\times):\ N_F = 4\,(\sin 45)\,C_{N_F} QS_F = 2.83\,C_{N_F} QS_F \tag{14}$$

An LV can be considered dynamically stable if, after being disturbed from a nominal trajectory, it oscillates about the nominal condition with an amplitude that decreases with time. A quantitative measure of dynamic stability or instability is the time it takes a disturbance motion to damp to half of its initial amplitude in a stable vehicle, or the time it takes for the initial amplitude to double in an unstable vehicle. The dynamic stability tests were conducted on three selected FCAs to determine qualitative dynamic stability characteristics. From the basic equations of motion (developed in references such as 12 or 13), it can be derived that

$$(t_{\text{half}} \text{ or } t_{\text{double}}) = \frac{2\,\ell n 2}{m_q + m_{\dot{\alpha}} + (z_\alpha/u)} \tag{15}$$

where

$$(m_q + m_{\dot{\alpha}}) = \frac{\left(C_{m_q} + C_{m_{\dot{\alpha}}}\right) QSd^2}{2uI_y}$$

and

$$z_\alpha = \frac{\left(C_{N_\alpha} + C_{D_o}\right) QS}{\text{mass}}$$

The natural frequency is a function of the pitching moment gradient, and the damping ratio is a function of both the pitching moment gradient and the pitch damping. Pitch damping wind tunnel test results are shown in Fig. 9 for the vehicle with no FCAs and with the three selected FCAs at four Mach numbers and forward c.g. Figure 10 shows qualitative results for the short-period mode approximation. It can be seen that the pitch damping increases significantly with the use of FCAs, for all FCAs and Mach numbers tested. It can also be seen that the time to half amplitude decreases significantly with the use of FCAs, for all FCAs and Mach numbers tested.

## Conclusion

The static flight stability analysis has shown that dramatic improvements in flight stability are achieved with the use of all the aft FCA designs. The experimental LV longitudinal stability improvements ranged from 41 to 72%, the 72% being achieved by the blunt-trailing-edgedesign. The control analysis showed that the mere presence of the FCAs, with no deflection, increased the control ratio by 46%. When FCA deflection was utilized, the control ratio increased by 110% for 3-deg FCA deflection to 346% for 6-deg FCA deflection, and at 9.1-deg FCA deflection the aerodynamic moment was completely trimmed. The canards were able to trim the vehicle at 5-deg deflection. The dynamic flight stability analysis has shown significant improvements in both the pitch damping and the short-period mode characteristics of the vehicle with the use of the designed blunt-trailing-edge FCAs at all Mach numbers tested.

## Acknowledgments

The author wishes to thank the Center Director's Discretionary Fund Program at the Marshall Space Flight Center (MSFC) for research funding and the wind tunnel test team at MSFC for its efforts.

## References

[1]Barret, C., "Launch Vehicle Flight Control Augmentation Using Smart Materials and Advanced Composites (CDDF Project 93-05 Part I)," NASA TP-3535, Feb. 1995.

[2]Barret, C., "Review of Our National Heritage of Launch Vehicles Using Aerodynamic Surfaces and Current Use of These by Other Nations (CDDF Project 93-05 Part II)," NASA TP-3615, April 1996.

[3]Barret, C., "Aerodynamic Flight Control Augmentation Devices for Saturn Class Launch Vehicles with Aft Centers-of-Gravity," *NASA Tech Briefs*, Vol. 19, No. 5, 1995, p. 99.

[4]Barret, C., "Launch Vehicle Shape Memory Alloy Actuators for Flight Control Augmentation Devices," *NASA Tech Briefs*, Vol. 19, No. 8, 1995, p. 79.

[5]Barret, C., "Flight Control Augmentation for Aft Center-of-Gravity Launch Vehicles," *Technology for the Stars*, NASA Marshall Space Flight Center Annual Rept., NASA TM-108501, 1995.

[6]Barret, C., "Flight Control Augmentation for Aft CG Launch Vehicles," AIAA Paper 96-0905, Jan. 1996.

[7]U.S. Air Force, *U.S. Air Force Stability and Control DATCOM*, Flight Control Div., U.S. Air Force Flight Dynamics Lab., Wright–Patterson AFB, OH, 1975.

[8]Wood, R. M., and Miller, D. S., "Impact of Airfoil Profile on Supersonic Aerodynamics," *Journal of Aircraft*, Vol. 23, No. 9, 1986, pp. 675–702.

[9]Ceresuela, R., "Aerodynamic Problems of Sounding Rockets," *AIAA Sounding Rocket Specialist Conference Proceedings*, AIAA, New York, 1967, pp. 73–83.

[10]Springer, A., "The MSFC's 14 × 14 Inch Trisonic Wind Tunnel," AIAA Paper 94-0539, Jan. 1994.

[11]Orlik-Ruckemann, K. J., "Techniques for Dynamic Stability Testing in Wind Tunnels," Dynamic Stability Parameters Conf., AGARD-CP-235, May 1978.

[12]Etkin, B., *Dynamics of Flight—Stability and Control*, 3rd ed., Wiley, New York, 1996, pp. 28–30.

[13]Nelson, R. C., *Flight Stability and Automatic Control*, 1st ed., McGraw–Hill, New York, 1989, Chaps. 2–5.

J. A. Martin
*Associate Editor*